

# Hypergraph-based Zero-shot Multi-modal Product Attribute Value Extraction

Anonymous Author(s)

## Abstract

It is essential for e-commerce platforms to provide accurate, complete, and timely product attribute values, in order to improve the search and recommendation experience for both customers and sellers. In the real-world scenario, it is difficult for these platforms to identify attribute values for the newly introduced products given no similar product history records for training or retrieval. Besides, how to jointly learn the product representation given various product information in multiple modalities, such as textual modality (e.g., product titles and descriptions) and visual modality (e.g., product images), is also a challenging task. To address these limitations, we propose a novel method for extracting multi-label product attribute-value pairs from multiple modalities in the zero-shot scenario, where labeled data is absent during training. Specifically, our method constructs heterogeneous hypergraphs, where product information from different modalities is represented by different types of nodes, and the text and image nodes are embedded and learned through CLIP encoders to effectively capture and integrate multi-modal product information. Then, the complex interrelations among these nodes are modeled through the hyperedges. By learning informative node representations, our method can accurately predict links between unseen product nodes and attribute-value nodes, enabling zero-shot attribute value extraction. We conduct extensive experiments and ablation studies on several categories of the public MAVE dataset and the results demonstrate that our proposed method significantly outperforms several state-of-the-art generative model baselines in multi-label, multi-modal product attribute value extraction in the zero-shot setting.

## Keywords

Attribute value extraction, Multi-modal learning, Zero-shot learning, Heterogeneous hypergraph

## 1 Introduction

Product attribute values are crucial in e-commerce as they provide valuable product information that enables customers to search, compare, and purchase their desired products more effectively and efficiently. Moreover, these values assist sellers in accurately representing and categorizing their products [59]. However, manual labeling by sellers often leads to incomplete or mislabeled attribute values, which could impede the searching and purchasing process for customers. To address these challenges, product attribute value extraction (AVE), which aims to automatically extract attribute values from product information, such as product titles, descriptions, and images, is an important task in the e-commerce field [59].

Most existing approaches for AVE rely on traditional supervised learning models, which require large quantities of labeled training data. However, manually labeling new products is often time-consuming and labor-intensive [16]. Consequently, it is essential to extract unseen attribute values for new products where labeled

training data is unavailable (i.e., in the zero-shot setting). In addition, many existing works focus on extracting attribute values from solely textual information, such as product titles and descriptions [39, 45, 46]. In real life, substantial attribute value information is implicitly contained within visual modality (i.e., product images), which is often overlooked compared to more explicit textual information [40, 52]. For instance, Figure 1 gives an example of the product data in our dataset, which includes both textual information, such as the product title and description, as well as visual information in the form of a product image. Moreover, though existing



Figure 1: An example of a product profile, including both textual and visual information.

SOTA generative multi-modal large language models (MLLMs) (i.e. LLaVA [28], Qwen [1], etc.) can handle multi-modal data input for a zero-shot attribute value prediction, these approaches are typically limited to generating a single attribute value at a time, lacking the capability to simultaneously extract multiple attribute-value pairs. This limitation is impractical for real-world applications, where products often possess several attribute-value pairs. Efficient extraction of these attribute values simultaneously is crucial for saving computational resources and reducing computational time.

To tackle the above challenges, we propose a hypergraph-based model for multi-modal, multi-label attribute value extraction in the zero-shot setting. Our model employs heterogeneous hypergraphs to capture intricate, higher-order interrelations among various types of nodes. These interrelations are derived from different aspects of product information or are influenced by user behaviors. Subsequently, the learned hypergraphs are capable of inferring connections between unseen product nodes and attribute value nodes. Specifically, we introduce four types of nodes, each representing products (i.e., product titles and descriptions), product categories, product attribute values, and product images. We first construct graphs to capture initial correlations and interactions

among these nodes; based on these graphs, we then construct a unified hypergraph to further capture more complex and higher-order interrelations influenced by user behaviors (i.e., ‘also view’, ‘also buy’) and product inventory information (e.g., ‘product with all images’) between nodes. The final node representations learned from the hypergraph encapsulate accurate and expressive information regarding products and product attribute values, demonstrating excellent capabilities in predicting links between new products and unseen attribute values. We conduct extensive experiments across 8 different product categories within the MAVE dataset, and the results indicate that our multi-modal hypergraph-based AVE model outperforms several existing methods in the zero-shot setting from the perspective of prediction performance and computational efficiency (time, GPU usage, and model weight). Furthermore, ablation studies show that integrating the visual modality can significantly improve the effectiveness of our model while introducing the hypergraph module also substantially improves the model performance compared to directly inferring from graphs.

Our main contributions are summarized as follows:

- We propose a zero-shot multi-modal, multi-label model to extract unseen attribute values for new products, which integrates an CLIP encoder to better learn the representations for both textual and visual product input data.
- We construct heterogeneous hypergraphs to capture complex and higher-order correlations and interactions from basic product information and user behavior information.
- Extensive experiments on the public dataset MAVE indicates that our proposed model significantly outperforms (higher F1-score and better computational efficiency) several SOTA generative MLLMs in zero-shot learning.

## 2 Related Work

### 2.1 Attribute Value Extraction

Product attribute value extraction aims at identifying attribute values based on the product information. Taking advantage of pre-trained large language models (LLMs), most existing studies focus on extracting attribute values from product titles or descriptions by using classification models [11, 12, 15], transformers [6], and generative LLMs [2, 14, 24, 34, 35, 37]. Some recent works explore the product visual features to enhance the product attribute value extraction by utilizing multi-modal transformer [40], combining OCR [27], using multi-modal attention mechanism [10, 52], prompt-tuning of pre-trained transformer [47], and directly leveraging multi-modal large language models (MLLMs) [56, 57] to generate product attribute values from the combination of product texts and images. However, these methods utilizing large (multi-modal) language models require large quantities of labeled training data for fine-tuning the pre-trained MLLMs. Even the works directly use the SOTA pre-trained MLLMs (i.e. Qwen [1], LLaVA [28]) for zero-shot attribute value generation still require computing resources for model inference [56] and demonstrate limited multi-label attribute value generation shown in Sec. 5.1. Besides, these works also miss the complex interrelations among different products. For multi-label zero-shot attribute value extraction, the most related work explores using heterogeneous hypergraph to do inductive link

prediction [17]. Nevertheless, it only considers text modality and misses the rich information and correlations from product images.

### 2.2 Multi-modal Zero-shot Learning

Multi-modal zero-shot learning (MZSL) has been widely applied in computer vision and natural language processing [5]. MZSL can be roughly divided into three main categories: (1) embedding-based methods, where the model directly constructs the mapping relationship between visual space and semantic space. One popular approach is the contrastive learning for MZSL [21] (i.e. CLIP [33], SigLIP [51], DreamLIP [54], etc.); (2) generative models, where ZSL is treated as a data-missing problem and representations of data in one modality is generated from another modality. For example, conditional variational autoencoders [31] or generative adversarial networks [18] are used to be trained on seen classes and then infer the characteristics of unseen classes in MZSL; (3) graph-based methods, where relationships between different classes and modalities are captured by graph links [4, 30, 43]. We propose to combine the embedding-based and graph-based approaches to leverage the strengths of both for MZSL on attribute value extraction.

### 2.3 Multi-modal Graph Learning

Although many current multi-modal learning techniques concentrate on mapping or aligning various modalities, real-world data is often more intricate, featuring complex many-to-many relationships that can be effectively modeled using graphs. Multi-modal graph learning (MGL) aims to tackle this complexity by leveraging graph structures with relational representations to fully explore both the inter-modal and intra-modal correlations from multi-modal data among multiple multi-modal neighbors [13, 32, 55]. Recent works in MGL have focused on integrating multi-modal features with graph or hypergraph structures (i.e. MGCN [22, 42], MGAN [23, 53], MGCL [25, 29], MHN [19, 49, 50]) across a wide range of downstream tasks (i.e. knowledge graph completion [36, 38, 41], recommendation [3, 19, 29], disease prediction [23, 44], etc.). Motivated by multi-modal fusion for hypergraphs with contrastive learning [19, 49] and the zero-shot ability from inductive link prediction in graphs [17], we propose a multi-modal hypergraph-based model with text and image nodes embedded through the CLIP encoder for zero-shot attribute value extraction in e-Commerce.

## 3 Methodology

### 3.1 Problem Formulation

In this section, we formally formulate the problem of heterogeneous hypergraph-based multi-modal zero-shot AVE, and provide some annotations for it. *The problem formulation is based on [16].* The product profile consists of product title and description, category, attribute values, and images. We denote a product profile as  $D = (P_t, P_o)$ , where  $P_t$  is the textual modality of the product profile and  $P_o$  is the visual modality. For the textual modality,  $P_t = (p_t^d, p_t^c, p_t^a)$ , where  $p_t^d$ ,  $p_t^c$ ,  $p_t^a$  represent product title and description, product category, and product attribute value, respectively. For the visual modality,  $P_o = (p_o^i)$ , where  $p_o^i$  represents product image.

Note that each product may have multiple images captured from different angles or perspectives to provide a comprehensive representation of its attributes and corresponding values. As illustrated in Figure 2, the product ‘cat bowl’ is depicted with three product images, each suggesting distinct attribute value information from different perspectives. For example, the top-left image demonstrates the design details of the cat bowl, the top-right image highlights its capacity, and the bottom image indicates that the bowl is specifically intended for cats. Also, each product may belong to multiple categories and have multiple attribute values. Still taking the cat bowl as an example, it is classified under categories such as Pet Supplies, Cats, and Bowls & Dishes, and has multiple attribute values, including Type: Pet Dish and Pet: Cat.

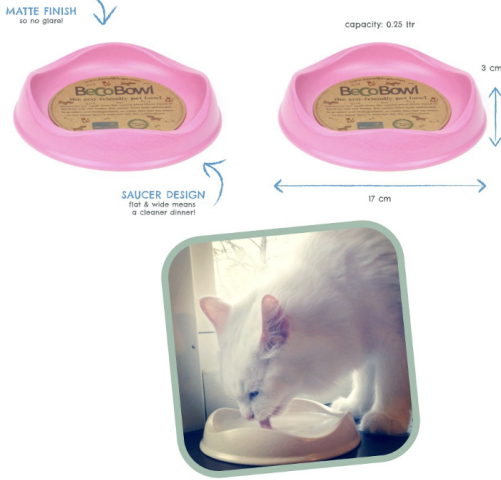


Figure 2: A product, Cat Bowl, with multiple images.

Given a product profile  $D$ , the goal of zero-shot AVE is to determine whether there is a link between a new product  $p$  and unseen attribute values  $p_t^a$ . The likelihood of such a link is calculated by the cosine similarity between  $p$  and  $p_t^a$ .

### 3.2 Model Overview

Figure 3 presents the overall framework of our proposed method. Essentially, our framework is composed of three main components: heterogenous hypergraph construction, hypergraph relation learning, and zero-shot link prediction. The details of each component are as follows:

**3.2.1 Heterogeneous Hypergraph Construction.** *Product inventory* refers to structured data that provides information about the attributes and characteristics of a product. In our context, product inventory data includes product titles and descriptions, product attribute values, product categories, and product images. *User behavior information* in e-commerce refers to the actions and activities that reflect how customers interact with e-commerce platforms, offering valuable insights into how certain products relate to others. In our case, we focus on two types of user behavior information: ‘also view’ and ‘also buy’. The ‘also view’ behavior means people

who view product A also view product B, and the ‘also buy’ behavior means people who buy product A also buy product B.

To enable hypergraphs to effectively capture correlations and interactions between product inventory data and user behavior information, we begin by constructing *graphs* that will serve as the basis for hypergraph construction. For graph construction, we define four types of nodes: *Products* ( $P$ ), *Categories* ( $C$ ), *Attribute Values* ( $A$ ), and *Images* ( $I$ ). To generate initial node representations, we employ the text encoder from the CLIP model [33] to encode textual information for  $P$ ,  $C$ , and  $A$ , while utilizing the CLIP image encoder to encode visual information for  $I$ . The initial node representations for  $P$ ,  $C$ ,  $A$ , and  $I$  are formulated as follows:

$$h_p = \text{CLIP}_{\text{text}}(p_t^d) \quad (1)$$

$$h_c = \text{CLIP}_{\text{text}}(p_t^c) \quad (2)$$

$$h_a = \text{CLIP}_{\text{text}}(p_t^a) \quad (3)$$

$$h_i = \text{CLIP}_{\text{image}}(p_o^i) \quad (4)$$

To establish connections between nodes, we introduce three types of edges: *product in category*, *product has attribute values*, and *product has images*. We formally define the edge set as:

$$E = \{e^{pc}, e^{pa}, e^{pi}\} \quad (5)$$

where  $e^{pc}$  denotes *product in category* edge,  $e^{pa}$  denotes *product has attribute values* edge,  $e^{pi}$  denotes *product has images* edge. Figure 3 Stage 1 demonstrates the graph construction process. By integrating these three subgraphs, we obtain a unified graph that encapsulates all relevant information from the product inventory.

The bottom part in Figure 3 Stage 1 demonstrates the process of *hypergraph construction* based on the information contained within the unified graph. We introduce two primary types of hyperedges, *also view* and *also buy*, which represent the previously described user behavior information. *also view* and *also buy* hyperedges capture the relationships between products and product images that align with the same user behavior. Additionally, we introduce another type of hyperedge, *product with all images*, which records the relationships between products and their corresponding images. Formally, we define the hyperedge set as:

$$\mathcal{E} = \{\epsilon^{vp}, \epsilon^{vi}, \epsilon^{bp}, \epsilon^{bi}, \epsilon^{pi}\} \quad (6)$$

where  $\epsilon^{vp}$  denotes *product also view* hyperedge,  $\epsilon^{vi}$  denotes *image also view* hyperedge,  $\epsilon^{bp}$  denotes *product also buy* hyperedge,  $\epsilon^{bi}$  denotes *image also buy* hyperedge, and  $\epsilon^{pi}$  denotes *product with all images* hyperedge. As shown in Figure 3 Stage 1, we use a single *also view* hyperedge to join multiple products that are viewed by the same user, and a single *also buy* hyperedge to join multiple products that are purchased by the same user. Additionally, images associated with the joined products are also connected using hyperedges of the same type. By doing this, we aim to exploit implicit correlated interrelations between products and images that may initially appear unrelated. Furthermore, a single *product with all images* hyperedge is utilized to connect each product with its corresponding images, facilitating the capture of interactions between the textual and visual modalities.

**3.2.2 Hypergraph Relation Learning.** By leveraging the structural information of the heterogeneous hypergraph (as shown in Figure 3 Stage 1), we perform hypergraph relation learning to fully identify

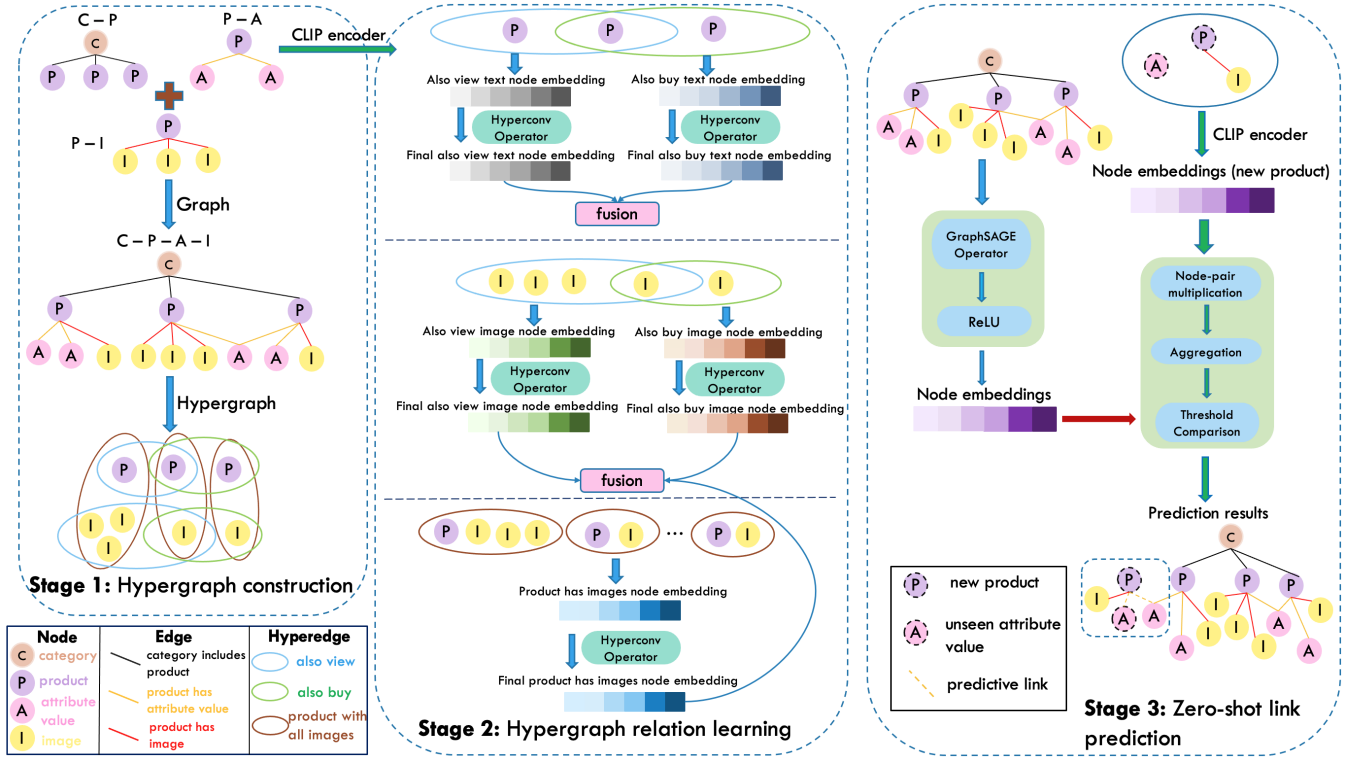


**Figure 3: Overview of our proposed model architecture. The model is composed of three main components: (1) Hypergraph construction: constructs hypergraphs based on product inventory data and user behavior information. (2) Hypergraph relation learning: captures higher-order relationships between product nodes and image nodes. (3) Zero-shot link prediction: infers links between new products and unseen attribute values.**

and understand the relationships between different entities within the heterogeneous hypergraph. Based on the initial node embeddings obtained from the CLIP text and image encoders, we conduct *message passing* within hypergraphs to enable more complex and informative node representations by aggregating information from neighboring nodes. For example, when calculating higher-order node representations for product nodes (as shown in the upper section in Figure 3 Stage 2), our model performs message passing:

$$m_{N(p_v)}^{(l)} = \text{AGGREGATE}^{(l)}(h_{p_u}^{(l)}, \forall u \in N(p_v)) \quad (7)$$

$$h_{p_v}^{(l+1)} = \text{UPDATE}^{(l)}(h_{p_v}^{(l)}, m_{N(p_v)}^{(l)}) \quad (8)$$

where  $h_{p_u}^{(l)}$  represents the embeddings of the neighboring nodes of node  $p_v^{(l)}$ ,  $h_{p_v}^{(l)}$  represents the embedding of the current node  $p_v^{(l)}$ , AGGREGATE is an aggregation function that aggregates the messages from the neighboring nodes, and UPDATE function is used to update the node embedding for node  $p_v^{(l)}$  based on its current features and the aggregated messages. Similarly, message passing for image nodes is calculated as follows:

$$m_{N(i_v)}^{(l)} = \text{AGGREGATE}^{(l)}(h_{i_u}^{(l)}, \forall u \in N(i_v)) \quad (9)$$

$$h_{i_v}^{(l+1)} = \text{UPDATE}^{(l)}(h_{i_v}^{(l)}, m_{N(i_v)}^{(l)}) \quad (10)$$

where  $h_{i_u}^{(l)}$  represents the embeddings of the neighborhood nodes of image node  $i_v^{(l)}$ ,  $h_{i_v}^{(l)}$  represents the embedding of the current image node  $i_v^{(l)}$ . We use the same AGGREGATE function and UPADTE function as previously defined.

When nodes belong to different modalities (i.e., both  $h_{p_v}^{(l)}$  and  $h_{i_v}^{(l)}$ ) within the hypergraph (as shown in the lower section of Figure 3 Stage 2), message passing is performed in the same manner. Message passing between nodes of different modalities enables the initial fusion of textual and visual features.

*Multi-modal Fusion.* After obtaining individual node embeddings for the five different types of hyperedges, we fuse the product node embeddings to generate a final unified node representation of products, and similarly, fuse the image node embeddings to create a final unified node representation for images. Moreover, different types of hyperedges may contribute unequally to the final node representations [16]. Therefore, we employ a fusion approach to further fuse node embeddings. This fusion approach considers varying levels of contribution from each hyperedge type, thereby optimizing both the final node representations and overall model performance. For *product also view* and *product also buy* hyperedges, we conduct fusion as follows:

$$h_{p_v} = \alpha \cdot h_{p_v}^{vp} + (1 - \alpha) \cdot h_{p_v}^{bp} \quad (11)$$

where  $h_{p_a}^{pp}$  is *product also view* node embedding,  $h_{p_a}^{bp}$  is *product also buy* node embedding,  $\alpha$  is the weight of *product also view* node embedding,  $1 - \alpha$  is the weight of *product also buy* node embedding, and  $h_{p_a}$  is the final unified product embedding.

Similarly, for *image also view*, *image also buy*, and *product with all images* hyperedges, the fusion is calculated as:

$$h_{i_v} = \gamma \cdot h_{i_v}^{vi} + \delta \cdot h_{i_v}^{bi} + (1 - \gamma - \delta) \cdot h_{i_v}^{pi} \quad (12)$$

where  $h_{i_v}^{vi}$  is *image also view* node embedding,  $h_{i_v}^{bi}$  is *image also buy* node embedding,  $h_{i_v}^{pi}$  is *product with all images* node embedding,  $\gamma$ ,  $\delta$ ,  $1 - \gamma - \delta$  are weights of *image also view*, *image also buy*, *product with all images*, respectively, and  $h_{i_v}$  is the final unified image embedding. Through the above fusion process, we obtain final product and image embeddings that capture more sophisticated correlations within user behaviors and product inventory information across different types of nodes and hyperedges.

**3.2.3 Zero-shot Link Prediction.** The relation learning stage allows us to obtain higher-level node embeddings that capture more intricate correlations among user behaviors and product inventory for both products and images. Additionally, we incorporate category and attribute value nodes, which are encoded by the CLIP text encoder, into the final graph structure to support the task of zero-shot link prediction. To generate the final node embeddings, all nodes in the final graph are processed through  $L$  layers of GraphSAGE [20], followed by the ReLU activation function.

To predict whether there is a link between a new product  $p$  and an attribute-value pair  $a$ , we calculate the cosine similarity between their embeddings to evaluate the probability that product  $p$  will have the attribute value  $a$ . Specifically, for a given product  $p_i$  and attribute value  $a_i$ , the cosine similarity is calculated as follows:

$$S_c(\tilde{h}_{p_i}, \tilde{h}_{a_i}) = \frac{\tilde{h}_{p_i} \cdot \tilde{h}_{a_i}}{\|\tilde{h}_{p_i}\| \cdot \|\tilde{h}_{a_i}\|} \quad (13)$$

where  $\tilde{h}_{p_i}$  is the node embedding for the new product  $p_i$  and  $\tilde{h}_{a_i}$  is the node embedding for the unseen attribute-value pair  $a_i$ . As shown in Figure 3 Stage 3, we predict whether a link exists between the new product (in a dotted line) and the unseen attribute-value pair (also in a dotted line) based on the previously learned graph. We can also predict links between the new product and existing attribute-value pairs. We employ a binary cross-entropy loss to optimize the performance of our model:

$$L = \sum_{p_i \in P, a_j \in A} y^{p_i a_j} \cdot \log(S_c^{p_i a_j}) + (1 - y^{p_i a_j}) \cdot (1 - \log(S_c^{p_i a_j})) \quad (14)$$

where  $y^{p_i a_j}$  is the ground truth for product-attribute sample  $p_i a_j$ ,  $S_c^{p_i a_j}$  is the predicted probability of the same sample. In addition, we employ the strategy of negative sampling to help train the model.

## 4 Experiments

### 4.1 Dataset

We conduct extensive experiments on eight main categories (Industrial, Arts, Cellphones, Automotive, Office products, Pet, Grocery, and Tools) from the MAVE dataset [48], which which is a large e-Commerce dataset derived from Amazon Review Dataset. For

each category, we concatenate the 'title' and 'description' into a single column, which is subsequently used as product node features. We leverage the 'category\_a' field, which records multiple subcategories for each product. We clean raw attribute-value pairs data by eliminating duplicate values and erroneous values. We use one or more product images associated with each product as visual information and exclude products with no corresponding images.

To simulate the zero-shot scenario, we split the dataset into training, validation, and test sets, ensuring that no overlap exists between them, following the multi-label zero-shot sampling in [16]. This step is critical since it prevents data leakage between the training, validation, and test stages, thereby guaranteeing a rigorous zero-shot link prediction setting. Note that each time the model is trained, we randomly re-split the data into training, validation, and test sets. Accordingly, we report the overall data statistic in Table 1.

### 4.2 Baselines Setup

Our model is compared with four state-of-the-art (SOTA) generative MLLMs (Qwen-VL [1], LLaVA [28], BLIP2 [26], InternVL [7]) for implicit attribute value extraction [58] in the zero-shot setting. Detailed descriptions of baseline models are in Appendix A.

For each baseline model, we use a standardized prompt template structured as follows: "What is the <attribute names> of this product: <'product titles and description'>? Answer with the option from the given choices directly: <attribute values>. Answer:" For example, for a product in the *Pet* category, the prompt would be: "What is the Material of this product: [Title] All Glass Aquarium AAG1055 Tank, 55-Gallon? Answer with the option from the given choices directly: acrylic, glass, pine, plastic, resin, steel, wood. Answer:". For products with multiple attribute values, the generative baselines are implemented multiple times (one attribute each time). Providing a standardized prompt format ensures a fair comparison across all baseline models. In addition, we keep only those attributes that have six or more corresponding attribute values for baselines. We randomly sample 2k data points to evaluate the performance of each baseline model as the inference time for baselines is very long shown in Table 4. More details are discussed in Section 6.

### 4.3 Implementation

**Implementation Details.** We implement our model using PyTorch and train it on a single NVIDIA A100 GPU. During training, we optimize the model using the AdamW optimizer. We perform a grid search to identify the optimal hyperparameters, setting the batch size to 256, learning rate to  $5e^{-5}$ , weight decay to  $1e^{-6}$ , dropout rate to 0.5, and training epochs to 500, which lead to the best model performance. The hidden size for both the hypergraph convolutional operator and the GraphSAGE operator is set to 512. When sampling neighbors in hypergraphs, we sample 20 neighbors for each node and set the rate of negative sampling to 2. We also limit the maximum length of text sequences to 77, truncating any text sequences that exceed this maximum length. For our model and all ablation studies, we run 10 times using different random seeds. In addition, after evaluating the effects of different weight configurations on model performance, we set the value of  $\alpha$  to 0.5, and both  $\gamma$  and  $\delta$  to 0.3 to optimize the model's performance.

**Table 1: Data statistics of eight categories in the MAVE dataset.**

Category	Number of Nodes				Number of Edges			Number of Hyperedges				
	P	C	A	I	$e^{pc}$	$e^{pa}$	$e^{pi}$	$e^{op}$	$e^{bp}$	$e^{oi}$	$e^{bi}$	$e^{pi}$
Industrial	1594	332	593	5207	6611	2895	5207	182	691	740	2831	4612
Arts	5195	569	1023	19359	21858	9165	19359	851	1562	3000	5764	17532
Cellphones	7238	114	877	32636	23438	14905	32636	875	390	4258	2069	31880
Automotive	7768	534	863	24807	34508	13436	24807	895	47	3142	180	22558
Office products	7486	391	1726	26232	36456	15263	26232	2324	4139	11032	21111	24034
Pet	9577	401	1196	35407	43414	20860	35407	3524	1616	14953	7104	33096
Grocery	10652	666	2021	35046	43953	20890	35046	4152	8590	15881	33762	32572
Tools	20046	782	3519	74522	82277	42465	74522	4656	2421	21170	10906	69312

*Evaluation Metrics.* To better evaluate the performance of our proposed model and compare it with other baseline methods, we use the *micro-F1* score and *mAP* (*mean Average Precision*) as our evaluation metrics for both the main results and ablation studies. F1 score is the harmonic mean of precision and recall, and it effectively evaluates both the accuracy and completeness of predicted product attribute values, making it a suitable metric for evaluating product attribute extraction. Similarly, mAP combines both precision and recall. It also enables the performance evaluation across multiple classes of attributes and offers a comprehensive view of the model’s performance. For the main results, we report the results in the form of F1/mAP (%) averaging from 10 runs. For ablation studies, we report the results in the form of F1/mAP (%)  $\pm$  standard deviation.

## 5 Results

### 5.1 Main Results

We evaluate the performance of our model on eight categories of the MAVE dataset and compare it with four baseline methods. The main results are presented in Table 2. We can observe that:

(1) In terms of both F1 and mAP, our model significantly outperforms all baselines in 5 out of 8 categories. For the three categories, *Industrial*, *Cellphones*, and *Grocery*, BLIP2 and InternVL perform comparably to our model or demonstrate slight improvements in terms of F1 or mAP. This indicates the success and bright potential of hypergraph-based models over generative MLLMs in multi-modal multi-label zero-shot attribute value extraction.

(2) From both Table 1 and Table 2, it can be observed that larger categories, which have a greater number of nodes, edges, and hyperedges, tend to exhibit poorer performance compared to categories with fewer nodes and edges. For example, the *Tools* category, represented by larger size of graphs and hypergraph, demonstrates the lowest performance among all categories. We argue that this is due to the increased complexity and diversity of interrelations between nodes and edges/hyperedges in larger graphs or hypergraphs, making these interrelations more difficult to capture and resulting in lower model performance. We tend to explore better approaches to capture more complex interconnections among products to better support larger hypergraphs in future work.

(3) As discussed in Section 4.2, the prompt example already reveals the number of attributes and attribute name information to the baseline models. Therefore, these baseline models only need

to predict the values for the known attribute names. For example, when provided with the attribute name *Material*, the baseline models only need to select the correct attribute values from a predefined attribute value list: *acrylic, glass, pine, plastic, resin, steel, wood*. In contrast, our model does not have prior knowledge of the attribute names. It directly extracts attribute name and value pairs. For example, our model is expected to extract correct attribute-value pairs such as "*Material: acrylic*", "*Material: glass*", and "*Material: pine*". However, we never provide the potential number of attributes and attribute names for our proposed model to do the prediction. In short, all the generative MLLM baselines have both the attribute names and the number of labels as their prior knowledge. Even under these circumstances, our model consistently outperforms other baselines in most cases or demonstrates comparable performance. This highlights the model’s superior ability in zero-shot attribute-value pair extraction compared to other generative baseline models.

Note that for the baseline models, we also experiment with prompts that do not explicitly point out the attribute names. We directly ask: "*What are the attribute values of this product? Choose at least one from the given choices directly: Material: acrylic, Material: glass, Material: pine, Material: plastic, Material: resin, Material: steel, Material: wood*". After extensive experiments, we find that these baseline models exhibit little or even no ability to directly extract attribute-value pairs in the zero-shot setting, performing poorly in terms of both F1 and mAP. Therefore, we choose to provide the attribute names for all generative baselines to evaluate their ability to predict attribute values in the zero-shot scenario. (Attribute names are never provided to our hypergraph-based model.)

### 5.2 Ablation Study

To evaluate the effectiveness of different components of our model, we conduct ablation studies in the following two aspects: (1) removing the visual information (i.e., product images) while retaining only the textual modality, (2) excluding hypergraphs from the framework and utilizing only graphs. The results of ablation studies are shown in Table 3. *w/o images* refers to the model without visual information, and *w/o hypergraphs* refers to the model without the hypergraph component.

**Ablating the visual information.** To evaluate the effectiveness of product images on the model’s performance, we conduct a visual ablation experiment by removing the images from the input and utilizing only textual information (i.e. product titles and descriptions, attribute values, and categories). As shown in Table 3, with the

**Table 2: Results F1 / mAP (%) across eight categories in the MAVE dataset. The best performances are highlighted in bold.**

Methods	Industrial	Arts	Cellphones	Automotive
Qwen-VL	29.75 / 49.51	28.44 / 50.14	19.80 / 50.22	12.71 / 50.17
LLaVA	38.88 / 50.17	10.11 / 50.14	41.11 / 50.22	22.67 / 50.17
BLIP2	37.70 / 49.52	22.55 / 50.46	33.00 / 49.40	28.65 / 49.95
InternVL	<b>41.20</b> / 50.37	25.60 / 50.25	33.50 / 49.31	39.10 / 50.80
Our model	40.44 / <b>62.91</b>	<b>50.00</b> / <b>78.33</b>	<b>41.67</b> / <b>59.58</b>	<b>49.62</b> / <b>57.52</b>
Methods	Office products	Pet	Grocery	Tools
Qwen-VL	10.91 / 50.11	22.90 / 50.14	22.37 / 50.09	25.11 / 50.10
LLaVA	4.77 / 50.11	14.92 / 50.14	29.98 / 50.09	24.47 / 50.10
BLIP2	25.43 / 49.87	40.80 / 49.80	34.85 / 51.43	<b>32.15</b> / 50.78
InternVL	24.42 / 50.48	27.60 / 50.22	37.80 / <b>51.89</b>	26.50 / 51.07
Our model	<b>59.05</b> / <b>79.17</b>	<b>60.00</b> / <b>54.33</b>	<b>40.00</b> / 51.70	26.03 / <b>51.28</b>

**Table 3: Experimental results F1 / mAP (%) of the effectiveness of different components in our model across eight categories in the zero-shot setting. The best performances are highlighted in bold.**

Model components	Industrial	Arts	Cellphones	Automotive
Full model	<b>40.44 ± 0.01</b> / <b>62.91 ± 0.04</b>	<b>50.00 ± 0.00</b> / <b>78.33 ± 0.04</b>	<b>41.67 ± 0.06</b> / <b>59.58 ± 0.10</b>	<b>49.62 ± 0.01</b> / 57.52 ± 0.07
w/o images	21.75 ± 0.01 / 37.37 ± 0.06	14.30 ± 0.00 / 47.49 ± 0.01	36.65 ± 0.02 / 67.80 ± 0.03	30.83 ± 0.03 / <b>57.57 ± 0.04</b>
w/o hypergraphs	22.22 ± 0.00 / 14.44 ± 0.00	15.65 ± 0.01 / 59.40 ± 0.00	24.55 ± 0.01 / 53.08 ± 0.03	32.82 ± 0.03 / 46.61 ± 0.05
Model components	Office products	Pet	Grocery	Tools
Full model	<b>59.05 ± 0.04</b> / <b>79.17 ± 0.04</b>	<b>60.00 ± 0.00</b> / <b>54.33 ± 0.07</b>	<b>40.00 ± 0.34</b> / <b>51.70 ± 0.00</b>	<b>26.03 ± 0.03</b> / <b>51.28 ± 0.08</b>
w/o images	26.34 ± 0.00 / 54.19 ± 0.01	28.65 ± 0.01 / 46.40 ± 0.02	11.83 ± 0.04 / 41.66 ± 0.06	16.67 ± 0.00 / 40.71 ± 0.05
w/o hypergraphs	50.24 ± 0.02 / 53.45 ± 0.02	37.61 ± 0.08 / 33.94 ± 0.05	32.86 ± 0.01 / 46.47 ± 0.01	22.65 ± 0.07 / 16.57 ± 0.02

exception of a minor increase in mAP in the *Automotive* category, we observe significant decreases in both F1 and mAP across all eight categories when image input is excluded. These experimental results indicate that relying solely on textual information may lead to suboptimal model performance. The result also validates our assumptions that product images have essential semantic information and attribute values are implicitly contained within visual modality.

**Ablating the hypergraphs.** To evaluate the effectiveness of the hypergraph module within our framework, we directly employ constructed graphs without hypergraph construction. As shown in Table 3, removing the hypergraph module leads to a significant decrease in both F1 and mAP across all categories, demonstrating the effectiveness of hypergraphs in improving the model performance. We argue that this is due to the superior capacity of hypergraphs to capture more complex, higher-order interconnected relationships among different types of nodes, compared to the binary graphs. For example, the *product also view* hyperedge, captures potential interrelations among a variety of products that are likely to share similar attributes. While the binary graph, where edges connect only two nodes, cannot represent these intricate relationships among multiple products. Similarly, the *product with all images* hyperedge, which connects multiple images associated with the same product, also captures potential interrelations among images (i.e. multiple views or angles of the product) representing the same product more effectively.

### 5.3 Efficiency Study

To evaluate the efficiency of our model, we conduct efficiency studies in (1) time efficiency and (2) computational efficiency.

**Time efficiency.** Table 4 presents the inference times for our model and baseline models. From Table 4, we observe that overall, the inference time for our model on the testing set is much shorter than the time required by each baseline model. We conjecture that this is because: (1) For our hypergraph model, the inference process is not sequential. It calculates the cosine similarity between pairs of nodes in parallel for inductive link prediction. However, for generative MLLMs, it requires the model to generate the outputs (attribute values) sequentially. (2) These generative MLLM baselines have more parameters, which require more computations during inference, leading to longer processing times. (3) We can also observe that certain categories, such as Arts, Automotive, and Grocery, require longer inference times than others among baselines. We think that this is because these categories contain attributes with a large number of corresponding values, which increases the time needed to generate predictions. Remember that for generative MLLM baselines, we use a prompt to ask the model to select the correct value from all possible options. This process takes much longer time when the option set is larger. For example, the 'Type' attribute in the *Arts* category has over 500 values, which significantly increased the time required to predict the correct values, resulting in a longer average inference time. This indicates that it is hard for generative MLLM baselines to scale up for larger categories with large quantities of possible attribute values.

**Computational efficiency.** Table 5 presents the computational efficiency of our model and baseline models. We can observe that compared to generative-based models, which exhibit high GPU memory consumption for the inference stage, our model does not require GPU utilization during inference. We argue that this is

**Table 4: Inference time (in seconds) across eight categories for our proposed model and all generative MLLM baselines.**

Methods	Industrial	Arts	Cellphones	Automotive
Qwen-VL	6.5942	71.5344	5.6962	111.9875
LLaVA	5.6520	49.3384	5.3908	74.4775
BLIP2	4.0582	37.0216	3.9530	89.9124
InternVL	0.4360	3.0832	0.3932	9.4643
Our model	0.1527	0.3357	0.3344	0.3592
Methods	Office products	Pet	Grocery	Tools
Qwen-VL	5.6804	20.7792	47.4036	12.7758
LLaVA	4.4766	17.4042	27.9954	10.3977
BLIP2	3.5157	12.3729	21.0672	14.3280
InternVL	0.3352	1.2327	2.0250	2.4048
Our model	0.4938	0.5746	1.1097	1.0694

due to our model’s ability to perform zero-shot link prediction by generalizing to new product nodes and unseen attribute value nodes without full model retraining. Furthermore, in contrast to baseline models with billions of parameters, our model is more lightweight with only 117 million parameters, which contributes to its lower computational cost and the feasibility of inference running on CPUs instead of GPUs, which saves computational costs for potential deployment in e-Commerce platforms.

**Table 5: Computational efficiency during inference**

Model	GPU Usage	Model Parameters
Qwen-VL	20432MiB / 81920MiB	9.6 Billion
BLIP2	9747MiB / 81920MiB	3.94 Billion
LLaVA	32590MiB / 81920MiB	13 Billion
InternVL	10208MiB / 81920MiB	2.2 Billion
Our model	no GPU	117 Million

## 6 Analysis and Discussion

(1) Our model demonstrates an excellent capability for **multi-label** product attribute value extraction, allowing it to extract values for multiple types of attributes simultaneously. For example, it can extract several attribute-value pairs, such as *'Variety: peanut'*, *'Flavor: lightly salted'*, *'Preparation: roasted'*, in a single step for a given product. In contrast, baseline models are limited to single-label attribute value extraction, requiring separate prompts for each attribute type. For example, they need one prompt to extract *'peanut'* for *'Variety'* and another to extract *'lightly salted'* for *'Flavor'*. In the real-world scenario, products often possess a diverse range of attribute names and values, and extracting these individually would cost extra computational resources and increase processing and inference time. As a result, our model is capable of achieving a more efficient, comprehensive, and accurate extraction of product attributes, increasing its potential for scale-up deployment in practical applications.

(2) As illustrated in 4.2, we keep only those attributes that have six or more corresponding attribute values. The main reason for doing this is to ensure a fair comparison between our model and the baseline methods. To enable this fair comparison, we disclose the attribute name information in the prompts to the baseline models,

which then predict values for those known attribute names. For attributes with only a few corresponding values, such as one or two, the baseline models can simply select from a very limited set of attribute values without performing any actual prediction or extraction. This results in artificially inflated F1 or mAP scores. Therefore, it is necessary to exclude those attributes with very few values. After experimenting with different numbers, we choose 6 as the threshold to guarantee robust performance of the baseline models while maintaining fairness in the comparison between the baseline methods and our model.

(3) As discussed in Section 5.1, we observe that larger categories tend to demonstrate lower performance compared to those categories of smaller sizes. This is likely due to the increased complexity of interrelations within larger graphs and hypergraphs. We conduct experiments with different hyperparameter configurations and find that the performance for larger categories can be improved by increasing the batch size or training the model with more epochs. We recommend using these strategies to enhance the model performance when dealing with larger categories.

## 7 Conclusion and Future Work

In this paper, we propose a hypergraph-based model for multi-modal, multi-label product attribute value extraction in the zero-shot setting. We aim to extract previously unseen attribute values for new products, where no labeled data is available for training. Specifically, we construct multi-modal hypergraphs in which both product textual and visual information are represented as different types of nodes, enabling the model to capture semantic, complex, and higher-order correlations among product image, product text, and user behavior information. Using constructed hypergraphs, we perform zero-shot (inductive) link prediction to infer the existence of links between unseen product nodes and attribute value nodes. We conduct extensive experiments across eight primary categories on the MAVE dataset, where our model demonstrates superior performance (higher F1-score, shorter inference time, and lighter weight) over several state-of-the-art generative multi-modal large language models. For future work, we will (1) build dynamic hypergraphs using timestamps to consider the real-time market; (2) explore other approaches for constructing hyperedges.

## References

- [1] Jinze Bai, Shuai Bai, Shusheng Yang, Shijie Wang, Sinan Tan, Peng Wang, Junyang Lin, Chang Zhou, and Jingren Zhou. 2023. Qwen-vl: A frontier large vision-language model with versatile abilities. *arXiv preprint arXiv:2308.12966* (2023).
- [2] Ansel Blume, Nasser Zalmout, Heng Ji, and Xian Li. 2023. Generative models for product attribute extraction. In *Proceedings of the 2023 Conference on Empirical Methods in Natural Language Processing: Industry Track*. 575–585.
- [3] Mert Burabak and Tevfik Aytekin. 2024. SynerGraph: An Integrated Graph Convolutional Network for Multimodal Recommendation. *arXiv preprint arXiv:2405.19031* (2024).
- [4] Rui Cai, Shichao Pei, and Xiangliang Zhang. 2024. Zero-Shot Relational Learning for Multimodal Knowledge Graphs. *arXiv preprint arXiv:2404.06220* (2024).
- [5] Weipeng Cao, Yuhao Wu, Yixuan Sun, Haigang Zhang, Jin Ren, Dujuan Gu, and Xingkai Wang. 2023. A review on multimodal zero-shot learning. *Wiley Interdisciplinary Reviews: Data Mining and Knowledge Discovery* 13, 2 (2023), e1488.
- [6] Wei-Te Chen, Keiji Shinzato, Naoki Yoshinaga, and Yandi Xia. 2023. Does Named Entity Recognition Truly Not Scale Up to Real-world Product Attribute Extraction?. In *Proceedings of the 2023 Conference on Empirical Methods in Natural Language Processing: Industry Track*, Mingxuan Wang and Imed Zitouni (Eds.), Association for Computational Linguistics, Singapore, 152–159. <https://doi.org/10.18653/v1/2023.emnlp-industry.16>
- [7] Zhe Chen, Jianan Wu, Wenhai Wang, Weijie Su, Guo Chen, Sen Xing, Muyan Zhong, Qinglong Zhang, Xizhou Zhu, Lewei Lu, et al. 2024. Internvl: Scaling up vision foundation models and aligning for generic visual-linguistic tasks. In *Proceedings of the IEEE/CVF Conference on Computer Vision and Pattern Recognition*. 24185–24198.
- [8] Wei-Lin Chiang, Zhuohan Li, Zi Lin, Ying Sheng, Zhanghao Wu, Hao Zhang, Lianmin Zheng, Siyuan Zhuang, Yonghao Zhuang, Joseph E Gonzalez, et al. 2023. Vicuna: An open-source chatbot impressing gpt-4 with 90%\* chatgpt quality. See <https://vicuna.lmsys.org> (accessed 14 April 2023) 2, 3 (2023), 6.
- [9] Hyung Won Chung, Le Hou, Shayne Longpre, Barret Zoph, Yi Tay, William Fedus, Yunxuan Li, Xuezhi Wang, Mostafa Dehghani, Siddhartha Brahma, et al. 2024. Scaling instruction-finetuned language models. *Journal of Machine Learning Research* 25, 70 (2024), 1–53.
- [10] Alois De la Comble, Anuvabh Dutt, Pablo Montalvo, and Aghiles Salah. 2022. Multi-modal attribute extraction for e-commerce. *arXiv preprint arXiv:2203.03441* (2022).
- [11] Zhongfen Deng, Wei-Te Chen, Lei Chen, and S Yu Philip. 2022. Ae-smnsmc: Multi-label classification with semantic matching and negative label sampling for product attribute value extraction. In *2022 IEEE International Conference on Big Data (Big Data)*. IEEE, 1816–1821.
- [12] Zhongfen Deng, Wei-Te Chen, Lei Chen, and Philip S. Yu. 2022. AE-smnsmc: Multi-Label Classification with Semantic Matching and Negative Label Sampling for Product Attribute Value Extraction. In *2022 IEEE International Conference on Big Data (Big Data)*. 1816–1821. <https://doi.org/10.1109/BigData55660.2022.10020304>
- [13] Yasha Ektefaie, George Dasoulas, Ayush Noori, Maha Farhat, and Marinka Zitnik. 2023. Multimodal learning with graphs. *Nature Machine Intelligence* 5, 4 (2023), 340–350.
- [14] Chenhao Fang, Xiaohan Li, Zehong Fan, Jianpeng Xu, Kaushiki Nag, Evren Korpeoglu, Sushant Kumar, and Kannan Achan. 2024. Llm-ensemble: Optimal large language model ensemble method for e-commerce product attribute value extraction. In *Proceedings of the 47th International ACM SIGIR Conference on Research and Development in Information Retrieval*. 2910–2914.
- [15] Jiaying Gong, Wei-Te Chen, and Hoda Eldardiry. 2023. Knowledge-Enhanced Multi-Label Few-Shot Product Attribute-Value Extraction. In *Proceedings of the 32nd ACM International Conference on Information and Knowledge Management (Birmingham, United Kingdom) (CIKM '23)*. Association for Computing Machinery, New York, NY, USA, 3902–3907. <https://doi.org/10.1145/3583780.3615142>
- [16] Jiaying Gong and Hoda Eldardiry. 2024. Multi-Label Zero-Shot Product Attribute-Value Extraction. In *Proceedings of the ACM on Web Conference 2024*. 2259–2270.
- [17] Jiaying Gong and Hoda Eldardiry. 2024. Multi-Label Zero-Shot Product Attribute-Value Extraction. In *Proceedings of the ACM Web Conference 2024* (Singapore, Singapore) (WWW '24). Association for Computing Machinery, New York, NY, USA, 2259–2270. <https://doi.org/10.1145/3589334.3645649>
- [18] Ian Goodfellow, Jean Pouget-Abadie, Mehdi Mirza, Bing Xu, David Warde-Farley, Sherjil Ozair, Aaron Courville, and Yoshua Bengio. 2020. Generative adversarial networks. *Commun. ACM* 63, 11 (2020), 139–144.
- [19] Zhiqiang Guo, Jianjun Li, Guohui Li, Chaoyang Wang, Si Shi, and Bin Ruan. 2024. LGMRec: Local and Global Graph Learning for Multimodal Recommendation. In *Proceedings of the AAAI Conference on Artificial Intelligence*, Vol. 38. 8454–8462.
- [20] Will Hamilton, Zhitao Ying, and Jure Leskovec. 2017. Inductive representation learning on large graphs. *Advances in neural information processing systems* 30 (2017).
- [21] Zongyan Han, Zhenyong Fu, Shuo Chen, and Jian Yang. 2021. Contrastive embedding for generalized zero-shot learning. In *Proceedings of the IEEE/CVF conference on computer vision and pattern recognition*. 2371–2381.
- [22] Wentai Hou, Chengxuan Lin, Lequan Yu, Jing Qin, Rongshan Yu, and Liansheng Wang. 2023. Hybrid graph convolutional network with online masked autoencoder for robust multimodal cancer survival prediction. *IEEE Transactions on Medical Imaging* 42, 8 (2023), 2462–2473.
- [23] Matthias Keicher, Hendrik Burwinkel, David Bani-Harouni, Magdalini Paschali, Tobias Czempel, Egon Burian, Marcus R Makowski, Rickmer Braren, Nassir Navab, and Thomas Wandler. 2023. Multimodal graph attention network for COVID-19 outcome prediction. *Scientific Reports* 13, 1 (2023), 19539.
- [24] Aaron Levine, Connie Huang, Chenguang Wang, Eduardo Batista, Ewa Szymanska, Hongyi Ding, Hou Wei Chou, Jean-François Pessiot, Johannes Effendi, Justin Chiu, et al. 2024. Rakutenai-7b: Extending large language models for japanese. *arXiv e-prints* (2024), arXiv-2403.
- [25] Dongyuan Li, Yusong Wang, Kotaro Funakoshi, and Manabu Okumura. 2023. Joyful: Joint Modality Fusion and Graph Contrastive Learning for Multimodal Emotion Recognition. In *Proceedings of the 2023 Conference on Empirical Methods in Natural Language Processing*, Houda Bouamor, Juan Pino, and Kalika Bali (Eds.), Association for Computational Linguistics, Singapore, 16051–16069. <https://doi.org/10.18653/v1/2023.emnlp-main.996>
- [26] Junnan Li, Dongxu Li, Silvio Savarese, and Steven Hoi. 2023. Bliip-2: Bootstrapping language-image pre-training with frozen image encoders and large language models. In *International conference on machine learning*. PMLR, 19730–19742.
- [27] Rongmei Lin, Xiang He, Jie Feng, Nasser Zalmout, Yan Liang, Li Xiong, and Xin Luna Dong. 2021. PAM: Understanding Product Images in Cross Product Category Attribute Extraction. In *Proceedings of the 27th ACM SIGKDD Conference on Knowledge Discovery & Data Mining (Virtual Event, Singapore) (KDD '21)*. Association for Computing Machinery, New York, NY, USA, 3262–3270. <https://doi.org/10.1145/3447548.3467164>
- [28] Haotian Liu, Chunyuan Li, Qingyang Wu, and Yong Jae Lee. 2024. Visual instruction tuning. *Advances in neural information processing systems* 36 (2024).
- [29] Kang Liu, Feng Xue, Dan Guo, Peijie Sun, Shengsheng Qian, and Richang Hong. 2023. Multimodal graph contrastive learning for multimedia-based recommendation. *IEEE Transactions on Multimedia* 25 (2023), 9343–9355.
- [30] Massimiliano Mancini, Muhammad Ferjad Naeem, Yongqin Xian, and Zeynep Akata. 2022. Learning graph embeddings for open world compositional zero-shot learning. *IEEE Transactions on pattern analysis and machine intelligence* 46, 3 (2022), 1545–1560.
- [31] Ashish Mishra, Shiva Krishna Reddy, Anurag Mittal, and Hema A Murthy. 2018. A generative model for zero shot learning using conditional variational autoencoders. In *Proceedings of the IEEE conference on computer vision and pattern recognition workshops*. 2188–2196.
- [32] Ciyuan Peng, Jiayuan He, and Feng Xia. 2024. Learning on Multimodal Graphs: A Survey. *arXiv preprint arXiv:2402.05322* (2024).
- [33] Alec Radford, Jong Wook Kim, Chris Hallacy, Aditya Ramesh, Gabriel Goh, Sandhini Agarwal, Girish Sastry, Amanda Askell, Pamela Mishkin, Jack Clark, et al. 2021. Learning transferable visual models from natural language supervision. In *International conference on machine learning*. PMLR, 8748–8763.
- [34] Kalyani Roy, Pawan Goyal, and Manish Pandey. 2024. Exploring generative frameworks for product attribute value extraction. *Expert Systems with Applications* 243 (2024), 122850.
- [35] Kassem Sabeh, Mouna Kacimi, Johann Gamper, Robert Litschko, and Barbara Plank. 2024. Exploring Large Language Models for Product Attribute Value Identification. *arXiv preprint arXiv:2409.12695* (2024).
- [36] Bin Shang, Yinliang Zhao, Jun Liu, and Di Wang. 2024. Lafa: Multimodal Knowledge Graph Completion with Link Aware Fusion and Aggregation. In *Proceedings of the AAAI Conference on Artificial Intelligence*, Vol. 38. 8957–8965.
- [37] Keiji Shinzato, Naoki Yoshinaga, Yandi Xia, and Wei-Te Chen. 2023. A Unified Generative Approach to Product Attribute-Value Identification. In *Findings of the Association for Computational Linguistics: ACL 2023*, Anna Rogers, Jordan Boyd-Graber, and Naoaki Okazaki (Eds.), Association for Computational Linguistics, Toronto, Canada, 6599–6612. <https://doi.org/10.18653/v1/2023.findings-acl.413>
- [38] Yaoshan Song, Pinglei Sun, Haoyu Liu, Zhixu Li, Wei Song, Yanghua Xiao, and Xiaofang Zhou. 2024. Scene-Driven Multimodal Knowledge Graph Construction for Embodied AI. *IEEE Transactions on Knowledge and Data Engineering* (2024).
- [39] Qifan Wang, Li Yang, Bhargav Kanagal, Sumit Sanghai, D Sivakumar, Bin Shu, Zac Yu, and Jon Elsas. 2020. Learning to extract attribute value from product via question answering: A multi-task approach. In *Proceedings of the 26th ACM SIGKDD international conference on knowledge discovery & data mining*. 47–55.
- [40] Qifan Wang, Li Yang, Jingang Wang, Jitin Krishnan, Bo Dai, Sinong Wang, Zenglin Xu, Madian Khabsa, and Hao Ma. 2022. Smartave: Structured multimodal transformer for product attribute value extraction. In *Findings of the Association for Computational Linguistics: EMNLP 2022*. 263–276.
- [41] Xin Wang, Benyuan Meng, Hong Chen, Yuan Meng, Ke Lv, and Wenwu Zhu. 2023. TIVA-KG: A multimodal knowledge graph with text, image, video and audio. In *Proceedings of the 31st ACM International Conference on Multimedia*. 2391–2399.

- [42] Youze Wang, Shengsheng Qian, Jun Hu, Quan Fang, and Changsheng Xu. 2020. Fake news detection via knowledge-driven multimodal graph convolutional networks. In *Proceedings of the 2020 international conference on multimedia retrieval*. 540–547.
- [43] Likang Wu, Zhi Li, Hongke Zhao, Zhefeng Wang, Qi Liu, Baoxing Huai, Nicholas Jing Yuan, and Enhong Chen. 2023. Recognizing unseen objects via multimodal intensive knowledge graph propagation. In *Proceedings of the 29th ACM SIGKDD Conference on Knowledge Discovery and Data Mining*. 2618–2628.
- [44] Yujing Xia, Lin Liu, Tao Dong, Juan Chen, Yu Cheng, and Lin Tang. 2024. A depression detection model based on multimodal graph neural network. *Multimedia Tools and Applications* (2024), 1–17.
- [45] Huimin Xu, Wenting Wang, Xinnian Mao, Xinyu Jiang, and Man Lan. 2019. Scaling up open tagging from tens to thousands: Comprehension empowered attribute value extraction from product title. In *Proceedings of the 57th Annual Meeting of the Association for Computational Linguistics*. 5214–5223.
- [46] Jun Yan, Nasser Zalmout, Yan Liang, Christian Grant, Xiang Ren, and Xin Luna Dong. 2021. Adatag: Multi-attribute value extraction from product profiles with adaptive decoding. *arXiv preprint arXiv:2106.02318* (2021).
- [47] Li Yang, Qifan Wang, Jingang Wang, Xiaojun Quan, Fuli Feng, Yu Chen, Madian Khabsa, Sinong Wang, Zenglin Xu, and Dongfang Liu. 2023. MixPAVE: Mix-prompt tuning for few-shot product attribute value extraction. In *Findings of the Association for Computational Linguistics: ACL 2023*. 9978–9991.
- [48] Li Yang, Qifan Wang, Zac Yu, Anand Kulkarni, Sumit Sanghai, Bin Shu, Jon Elsas, and Bhargav Kanagal. 2022. Mave: A product dataset for multi-source attribute value extraction. In *Proceedings of the fifteenth ACM international conference on web search and data mining*. 1256–1265.
- [49] Zijian Yi, Ziming Zhao, Zhishu Shen, and Tiejua Zhang. 2024. Multimodal Fusion via Hypergraph Autoencoder and Contrastive Learning for Emotion Recognition in Conversation. *arXiv preprint arXiv:2408.00970* (2024).
- [50] Yawen Zeng, Qin Jin, Tengfei Bao, and Wenfeng Li. 2023. Multi-modal knowledge hypergraph for diverse image retrieval. In *Proceedings of the AAAI Conference on Artificial Intelligence*, Vol. 37. 3376–3383.
- [51] Xiaohua Zhai, Basil Mustafa, Alexander Kolesnikov, and Lucas Beyer. 2023. Sig-moid loss for language image pre-training. In *Proceedings of the IEEE/CVF International Conference on Computer Vision*. 11975–11986.
- [52] Yupeng Zhang, Shensi Wang, Peiguang Li, Guanting Dong, Sirui Wang, Yunsen Xian, Zhoujun Li, and Hongzhi Zhang. 2023. Pay attention to implicit attribute values: a multi-modal generative framework for AVE task. In *Findings of the Association for Computational Linguistics: ACL 2023*. 13139–13151.
- [53] Zhenrong Zhang, Jiefeng Ma, Jun Du, Licheng Wang, and Jianshu Zhang. 2022. Multimodal pre-training based on graph attention network for document understanding. *IEEE Transactions on Multimedia* 25 (2022), 6743–6755.
- [54] Kecheng Zheng, Yifei Zhang, Wei Wu, Fan Lu, Shuailei Ma, Xin Jin, Wei Chen, and Yujun Shen. 2024. DreamLIP: Language-Image Pre-training with Long Captions. *arXiv preprint arXiv:2403.17007* (2024).
- [55] Jing Zhu, Yuhang Zhou, Shengyi Qian, Zhongmou He, Tong Zhao, Neil Shah, and Danai Koutra. 2024. Multimodal Graph Benchmark. *arXiv preprint arXiv:2406.16321* (2024).
- [56] Henry Zou, Vinay Samuel, Yue Zhou, Weizhi Zhang, Liancheng Fang, Zihe Song, Philip Yu, and Cornelia Caragea. 2024. ImplicitAVE: An Open-Source Dataset and Multimodal LLMs Benchmark for Implicit Attribute Value Extraction. In *Findings of the Association for Computational Linguistics ACL 2024*, Lun-Wei Ku, Andre Martins, and Vivek Srikumar (Eds.), Association for Computational Linguistics, Bangkok, Thailand and virtual meeting, 338–354. <https://doi.org/10.18653/v1/2024.findings-acl.20>
- [57] Henry Zou, Gavin Yu, Ziwei Fan, Dan Bu, Han Liu, Peng Dai, Dongmei Jia, and Cornelia Caragea. 2024. EIVEN: Efficient Implicit Attribute Value Extraction using Multimodal LLM. In *Proceedings of the 2024 Conference of the North American Chapter of the Association for Computational Linguistics: Human Language Technologies (Volume 6: Industry Track)*, Yi Yang, Aida Davani, Avi Sil, and Anoop Kumar (Eds.), Association for Computational Linguistics, Mexico City, Mexico, 453–463. <https://doi.org/10.18653/v1/2024.naacl-industry.40>
- [58] Henry Peng Zou, Vinay Samuel, Yue Zhou, Weizhi Zhang, Liancheng Fang, Zihe Song, Philip S Yu, and Cornelia Caragea. 2024. ImplicitAVE: An Open-Source Dataset and Multimodal LLMs Benchmark for Implicit Attribute Value Extraction. *arXiv preprint arXiv:2404.15592* (2024).
- [59] Henry Peng Zou, Gavin Heqing Yu, Ziwei Fan, Dan Bu, Han Liu, Peng Dai, Dongmei Jia, and Cornelia Caragea. 2024. EIVEN: Efficient implicit attribute value extraction using multimodal LLM. *arXiv preprint arXiv:2404.08886* (2024).

## A Baselines

Below are detailed descriptions of baseline models:

**Qwen-VL** [1] carefully designs a visual receptor, a position-aware vision-language adapter, and a three-stage training pipeline to optimize the entire model, enabling its superior visual understanding

ability. We evaluate the performance of the Qwen-VL model and present the results in the following section.

**BLIP2** [26] proposes an efficient framework that pre-trains a light-weight Querying Transformer in two stages. The first stage learns a vision-and-language representation leveraging a frozen image encoder, while the second stage performs vision-to-language generative learning leveraging a frozen LLM. We conduct experiments with BLIP-2 using FLAN-T5-XL [9] as the backbone LLM model.

**LLaVA** [28] connects the pre-trained visual encoder from CLIP with an LLM decoder Vicuna [8], fine-tuning on ChatGPT/GPT-4 generated vision-language instruction-following data to enable comprehensive visual and language understanding. We evaluate the performance of LLaVA with Vicuna-13B as the backbone LLM model.

**InternVL** [7] scales up the vision foundation model to 6 billion parameters and aligns it with the LLM through three progressive stages, including vision-language contrastive learning, vision-language generative training, and supervised fine-tuning, achieving powerful visual capabilities. We conduct experiments with the InternVL2-2B variant.